Sensors and Actuators: A. Physical xxx (2022) xxx

Current-induced degradation behaviors of InGaN/GaN multiple-quantum-well UV photodetectors: Role of electrically active defects

Pradip Dalapati[a,*], Abdulaziz Almalki[b,c], Sultan Alhassan[b], Saud Alotaibi[b], Maryam Al Huwayz[b], Taiki Nakabayashi[a], Takashi Egawa[a,d], Makoto Miyoshi[a,d], Mohamed Henini[b]

[a] Research Center for Nano-Devices and Advanced Materials, Nagoya Institute of Technology, Nagoya 466-8555, Japan

[b] School of Physics and Astronomy, University of Nottingham, Nottingham NG7 2RD, United Kingdom

[c] Physics Department, Faculty of Science at Taibah University-Yanbu, King Khalid Rd. Al Amoedi, 46423, Yanbu El-Bahr, 51000, Saudi Arabia

[d] Innovation Center for Multi-Business of Nitride Semiconductors, Nagoya Institute of Technology, Nagoya 466-8555, Japan

ABSTRACT- To examine the critical role of electrically active defects and surface states in InGaN/GaN multiple quantum well (MQW) ultraviolet photodetectors (UV-PDs), the study of degradation mechanisms in such devices is very important. In this work, we have fabricated InGaN/GaN MQW UV-PDs with a thick passivation layer of Al_2O_3 and studied their degradation behaviors by applying high current stress. The origin of degradation processes has been investigated intensively by employing different combined optical and electrical measurements. As a consequence of stress, we noticed that (i) the electroluminescence intensity decreases distinctly (~ 48%), suggesting that more of the charge carriers are captured by the newly induced defects in the active region; (ii) the open circuit voltage is mostly accountable for the degradation of photovoltaic properties in treated PDs; (iii) the parasitic current leakage paths increase significantly which in turn reduce the photocurrent generation process largely; (iv) within the temperature range of 100-440 K, the values of the ideality factor and barrier height are found to be always higher and lower in treated PDs, respectively, indicating the presence of generation-recombination centers caused by defects; (v) two major trap levels are identified in treated PDs via Laplace deep level transient spectroscopy analysis; and (vi) the responsivity in treated PDs decreases. The obtained results indicate that degradation is mainly associated with the newly generated defects, mostly Mg-related shallow acceptors, including Mg_{Ga} and Mg-H_2 complexes, which can form the acceptor levels as a result of the breaking of Mg-H chemical complexes due to high heating levels during the stress treatment.

* Corresponding author.

E-mail address: pradipdalapati@gmail.com (P. Dalapati).

Keywords: GaN-based photodetectors, degradation, trap levels, chemical nature, LDLTS.

1. Introduction

Nowadays, the advancement of wide bandgap semiconductors (GaN, AlGaInN, MgZnO, Ga_2O_3, $ZnGa_2O_4$, etc.) based ultraviolet photodetectors (UV-PDs) is one of the utmost in demand and extensively developed areas of optoelectronic devices because UV-PDs find widespread civilian, space, and military applications, including remote control systems, multispectral flame sensing, ozone monitoring, space communication systems, and missile warning systems [1-4]. However, several detrimental effects originating from native defects and surface states in such devices hinder the novel development of super-sensitive UV-PDs [5-8]. For the development of high-performance UV light detection devices with ultrafast response speed, InGaN/GaN multiple quantum well (MQW) structures have commonly been employed in Refs. [9-12]. The InGaN/GaN MQW structure can effectively decrease the thermodynamic and strain-induced structural instabilities as well as the formation of V-type defects, leading to surpassing the technical bottleneck in the usable high spectral responsivity [11,13].

Furthermore, the technological difficulties for the production of low defects and large area GaN substrates, propel the use of other less matching substrates, namely, Si and sapphire for the fabrication of PD. Therefore, the obvious lattice mismatch and the dissimilarity in thermal expansion coefficients between GaN and these substrates lead to the generation of large defects in InGaN/GaN heterostructures [14]. Several defects and structural imperfections in InGaN/GaN MQW PD play many critical roles for various unfavorable effects which strongly affect the photoexcited charge carrier separation process in PD.

The practical applications of such devices in numerous fields demand highly reliable and stable PDs. Therefore, for the development of highly stable UV-PDs, the role of surface states and high defect density, including threading dislocations (TDs) and native point defects need to be studied rigorously. In our earlier works [15,16], we reported the impact of constant current stress on the different electrical and optical properties of similar PDs and observed that the degradation processes are usually associated to the newly generated electrically active defects in the stressed devices. Based on X-ray diffraction (XRD) and X-ray photoelectron spectroscopy (XPS) results, Horng et al. [4] claimed that in $ZnGa_2O_4$-based deep ultra-violet (DUV) photodetectors, the main degradation is affected by the ozone compensation as well as the surface water adsorption. However, the defect-related degradation mechanisms in InGaN-based PDs are not well investigated until now. Several open questions remain unanswered: Where are the

central defect levels situated? How do they penetrate in the different epilayers? What is their chemical nature? What are their activities in the devices? Thereby, to fabricate high-efficiency and high-reliable InGaN-based UV-PDs, an in-depth inspection of the location of defects and their activities in such devices is importantly required.

To acquire detailed information regarding the above issues, we have investigated in the present work the degradation behaviors of the optical and electrical properties of InGaN/GaN MQW UV-PDs at high constant current stress. Before we portray the details of the study, we specify below certain essential and novel aspects of the present investigation. First, we have grown InGaN/GaN MQW UV-PD structure on sapphire substrate and fabricated devices with a 20-nm-thick Al_2O_3 passivation layer on the top which can reduce the surface states significantly. Second, we have obtained the optical and electrical characteristics of untreated and treated UV-PDs to understand the root mechanisms of the degradation. Third, we have acquired deep level transient spectroscopy (DLTS) and Laplace-DLTS spectra for the untreated and treated UV-PDs to identify the location as well as the nature of the electrically active defects. Finally, we have checked the effect of current stress on the sensitization performance of the detector.

2. Device fabrication and characterization

In the present work, an InGaN/GaN MQW UV-PD structure was grown on the *c*-plane of a sapphire substrate by using a horizontal metal organic chemical vapor deposition (MOCVD) system. The cross-sectional view of the employed PD structure is schematically displayed in Fig. 1. Initially, the low-temperature GaN (LT-GaN) buffer layer of 30 nm was grown on the substrate and then, a thick Si-doped *n*-type GaN layer (growth temperature (GT): 1160 °C, thickness: 2.5 μm, doping concentration ≈ 3×10^{18} cm^{-3}) was grown on LT-GaN layer. On the top of n-GaN layer, a large number (42-period) of InGaN/GaN (3/3 nm) MQW active region (GT: 825 °C) was prepared. After the MQW region, the top Mg-doped p-type GaN layers were grown by a two-step growth process. During the growth of the first 100 nm p-GaN layer, the value of GT was kept at 825 °C, whereas the remaining 150 nm p-GaN layer was grown at 875 °C. The Mg concentration for the p-GaN layers was about 5×10^{19} cm^{-3}. Furthermore, it is noted that the two-step growth process can improve the device performance significantly as observed in our recent work [17].

From the XRD data (see Supporting Information (Appendix A)), we calculated the value of In composition in the active region which was about 9%. In addition, the estimated value of the density of TDs was about 9.1×10^8

cm^{-2}. Before the device fabrication, we checked the surface morphology of the top GaN layer via atomic force microscopy (AFM) analysis (see Supporting Information (Appendix A)). The obtained value of the root mean square (RMS) roughness was 11.66 nm.

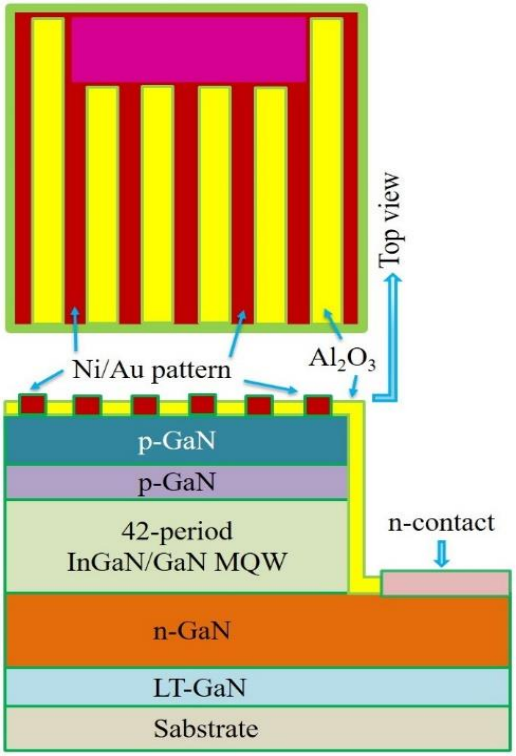

Fig. 1. Schematic illustration (cross-sectional) of InGaN-based UV-PD structure.

To fabricate UV-PDs, we followed the standard device fabrication techniques of a photolithographic method, BCl_3 plasma reactive ion etching (RIE), electron beam metal evaporation, and subsequent annealing processes. The photolithographic method was used to imprint the device structure on the epilayer, whereas the RIE was employed to etch the contact regions (n-type) of the device. After that the etched sample was annealed at 750 °C for 30 minutes in N_2 atmosphere to activate the Mg acceptors in the p-GaN layers. Following the Mg acceptors activation process, the n-contact was formed by depositing Ti/Al/Ni/Au (15/60/12/60 nm) metals using electron beam evaporation (EBE) process, whereas the finger-shaped p-contact was also deposited by the same process (EBE) with Ni/Au (5/60 nm) metals (see the top view in Fig. 1). Next, a rapid (30 s) annealing process at 750 °C in N_2 atmosphere was performed to accomplish good n-type Ohmic contact layers. In addition, to attain p-type Ohmic

contacts, the sample was annealed at 600 °C for 3 minutes in O_2 atmosphere. Before the finalization of PD fabrication, a 20-nm thick Al_2O_3 passivation layer was deposited on the sample (without contact electrodes) to reduce the effect of surface states. The passivation film was deposited by an atomic layer deposition unit (Cambridge Nano-tech) [18]. During the atomic layer deposition, trimethylaluminum was used as an Al precursor, whereas purified H_2O and O_3 were considered as the O_2 precursors [11,18]. However, the details of the various optical and electrical measurements (electroluminescence (EL), current-voltage (*I–V*) at different conditions (without and with light, low-temperature), dark capacitance–voltage (*C–V*), DLTS, and photocurrent spectroscopy (PCS)) are described in our earlier articles [11,15,17,19]. Furthermore, it is to be noted that in the present work, the constant high-current (200 mA) stress treatments of the un-encapsulated UV-PDs were performed at room temperature and open laboratory environment. On the other hand, the DLTS and LDLTS were carried out in the temperature range of 10 K-450 K using a Boonton 7200 capacitance meter, a pulse generator, a Lake Shore 331 temperature controller and a data acquisition system. All the PDs samples (two fresh and three treated) were mounted and wire-bonded onto TO5 headers and fitted in a Janis closed-loop helium cryostat for the temperature dependence measurements.

3. Experimental results and discussion

3.1. Degradation of luminescence property

We have recorded the degradation of luminescence property in our devices as these PDs contain a 42-period of InGaN/GaN MQW active region. Due to constant current stress at 200 mA over 340 hours, the EL intensity for the driving current of 100 mA decreased markedly (~ 48%) as depicted in Fig. 2. Ma et al. [19] suggested that in InGaN/GaN MQW structures, the hegemony of TDs ruins the luminescence property of the active region because these TDs act as non-radiative recombination centers (NRCs). However, the obtained results in Fig. 2 suggest that the degradation of EL intensity in the treated PDs is closely related to the newly created defects in the active region of the device where numerous charge carriers can recombine non-radiatively. These defects, therefore, reduce the EL intensity substantially [15]. Furthermore, it is to be mentioned that throughout the stress treatment, the full width at half maximum (FWHM) does not change significantly, whereas the MQW emission peak in the treated PD is shifted slightly from 412.2 nm (fresh PD) to 412.4 nm (see Fig. 2). This small red-shift could be due to

the In content fluctuation as suggested in Ref. [15]. In addition, the In fluctuation can affect the NRCs in the device as well. Therefore, this In fluctuation in the treated PDs can further reduce the EL intensity.

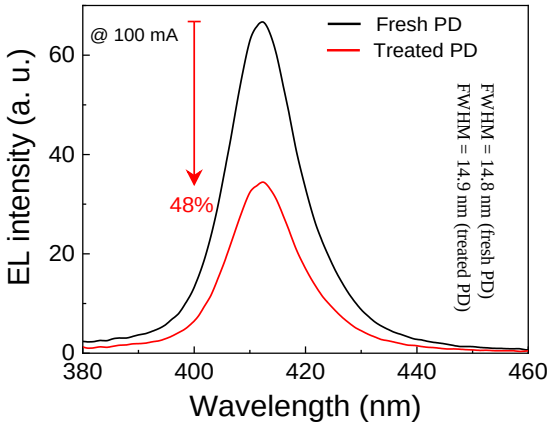

Fig. 2. EL spectra at 100 mA acquired before (black line) and after 340 hours of stress treatment (red line). FWHM: 14.8 nm (fresh PD), 14.9 nm (treated PD).

3.2. Degradation of photovoltaic properties

It is important to note that studies on the degradation of photovoltaic properties, namely, short circuit current density (J_{SC}) and open circuit voltage (V_{OC}) in InGaN/GaN MQW PDs under different stress conditions are not widely available in the literature [16,20,21]. However, to get a deep perception into the degradation of photovoltaic properties of InGaN-based PDs, we have measured *I–V* characteristics under the artificial solar light with a standard air-mass 1.5 global spectrum i. e., standard 1 sun-intensity (power density: 100 mW/cm^2) before and after 340 hours of stress treatment and the obtained results are illustrated in Fig. 3. It can be noticed in Fig. 3 that J_{SC} reduces slightly from 0.55 to 0.54 mA/cm^2 due to stress treatment. On the other hand, V_{OC} decreases from 2.11 V (fresh PD) to 1.1 V (treated PD), suggesting the defect-related forward conduction processes are increased due to stress (more details are mentioned in the next section) [21]. In InGaN/GaN MQW stressed solar cells, Caria et al. [21] observed that the reduction in V_{OC} is much higher than that of J_{SC}. In another work, Huang et al. [20] noticed the same trend of variation in V_{OC} and J_{SC} in similar stressed devices. These reports support our present observation in Fig. 3. Furthermore, this noteworthy decrease in V_{OC} seems to be the foremost degradation mechanism in our

devices. In our earlier work [16], we noticed that due to the strong resistive effects in treated PDs, the photovoltaic properties decrease significantly. To get additional information, we have calculated the values of shunt resistance (R_{SH}) and series resistance (R_S) for fresh and treated PDs from the obtained *I–V* results (under light). Interestingly, the value of R_{SH} decreases from 6850 (fresh PD) to 1070 kΩ, whereas R_S increases from 62 (fresh PD) to 117 kΩ. The high resistive effects in the treated PDs could be related to the activation of initially inactive defects [16]. Nevertheless, the strong reduction in R_{SH} as well as the improvement in the magnitude of R_S during the stress treatment might ruin the photovoltaic properties of the detector significantly as observed in Fig. 3.

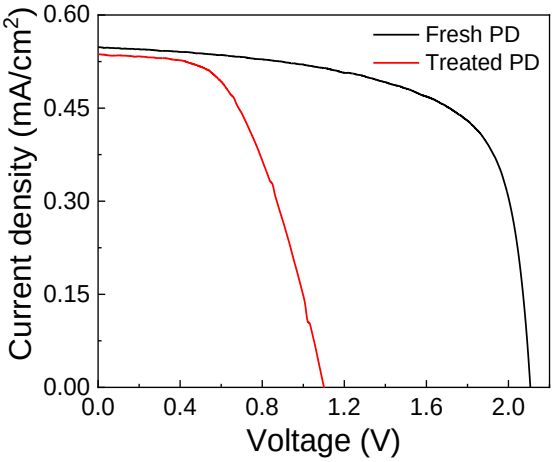

Fig. 3. *J–V* characteristics of fresh and treated PDs measured under standard 1 sun intensity at room temperature.

3.3. Dark I–V characteristics

We have acquired the dark *I–V* curves for fresh and treated PDs at room temperature and the achieved results are presented in Fig. 4. For the specific bias-dependent current transport analysis, three different regions, namely, I, II, and III are designated in Fig. 4. When our devices are subjected to the constant current stress, the reverse leakage current (region III) increases significantly, suggesting the parasitic leakage routes that are usually prompted by severe point defects within or around the MQW are activated strongly during the treatment [15]. It can be noticed in Fig. 4 that within 0 to 2 V (region II), the subturn-on forward leakage increases markedly in the treated PDs, indicating the defect-assisted mechanisms play a paramount role in the carrier transport. In this bias region, the

trap-assisted tunneling process can aid in the motion of numerous electrons and hence, increase the carrier leakage in the device [15]. Region I indicates that both the ideality factor (n) as well as R_S are increased in the treated PDs. It is interesting to note that in a high-forward bias (region I), the current flow through the treated PDs at a fixed forward voltage decreases slightly. This decrease of current could be due to the effect of high series resistance in the treated PDs. In addition, we have achieved a very good rectification ratio in fresh PD which is about 2.91×10^5 at ± 3.5 V. The rectification ratio at ± 3.5 V is defined as ratio between the diode currents measured at + 3.5 V and – 3.5 V, respectively. The value of rectification ratio reduces remarkably to 1.32×10^3 at ± 3.5 V due to long-time treatment. These quantitative results further support the observation of leakage current in treated PDs (Fig. 4).

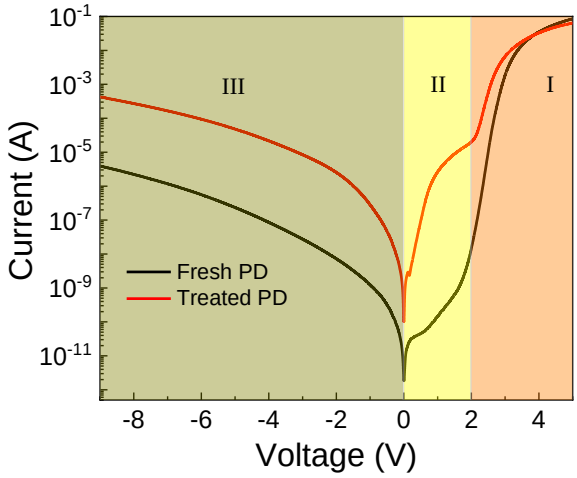

Fig. 4. *I–V* characteristics acquired before and after 340 hours of current stress treatments.

Furthermore, we have estimated the values of n and barrier height (ϕ_b) at different temperatures for both the PDs (fresh and treated) to gain further insight into the device physics. We have used the well-known Werner's method to determine the diodes parameters (n, and ϕ_b). The current-voltage characteristics of p-n junctions can be described by thermionic emission, as given below [22]:

$$I = I_s \left[exp\left(\frac{q(V - IR_S)}{nkT}\right) - 1 \right] \quad (1)$$

$$I_s = AA^* T^2 \, exp\left(\frac{-q\phi_b}{kT}\right) \quad (2)$$

where q is the elementary charge, k is Boltzmann's constant, T is the temperature, ϕ_b is the barrier height, A is the effective diode area, A^* is the effective Richardson's constant. The forward I–V characteristics for all samples are used to obtain the values of n, and ϕ_b. The estimated values of n and ϕ_b at different temperatures are plotted in Fig. 5a and b, respectively.

It should be noted that the value of n at room temperature increases from 2.20 ± 0.01 (fresh PD) to 3.87 ± 0.01 (treated PD), suggesting the generation of defects in or around the active region during the stressing process [23]. However, for both devices, it is evident that the ideality factor increases significantly due to lowering of temperature from 440 to 100 K (see. Fig. 5a). In this temperature range, the value of n increases from 1.4 to 12.6 for the untreated PD, whereas for treated PD, it rises from 2.71 to 20.86. Similar trends have also been reported previously [24-26]. This behaviour can be explained by a temperature-activated process due to the current transport across the junction interfaces [27,28]. In the temperature range of 300-440 K, both devices demonstrated values of n greater than unity and close to 2. A variety of factors may be responsible for this behaviour. These include generation-recombination mechanisms, interface states, series resistances, and barrier height inhomogeneities [24,29]. However, the fresh device has a lower value of n than the treated device, suggesting that the fresh device is closer to ideal diodes than the treated device. At low temperatures, the higher values of n indicate an additional mechanism to the pure thermionic emission that contributes to the current, namely the thermionic field emission [30]. Another possible reason for the deviation of n values from unity at low temperatures may be due to the presence of generation-recombination centers caused by defects in the GaN, such as deep levels in the forbidden gap [31].

Fig. 5b illustrates the temperature dependence of the barrier height for both devices. The barrier height increases linearly with increasing temperature (see the linear fits in Fig. 5b). However, the fresh device has a slightly larger barrier height than the treated device which can be attributed to current stress. The barrier height at 100 K and 440 K for the fresh and treated devices are 0.27 eV and 1.28 eV, and 0.23 eV and 1.24 eV, respectively. The lower value of ϕ_b in the treated PD suggests that numerous carriers might reach the defect states easily and enhance the

non-radiative recombination mechanism rather than their separation, resulting in a poor photocurrent generation process [15,16].

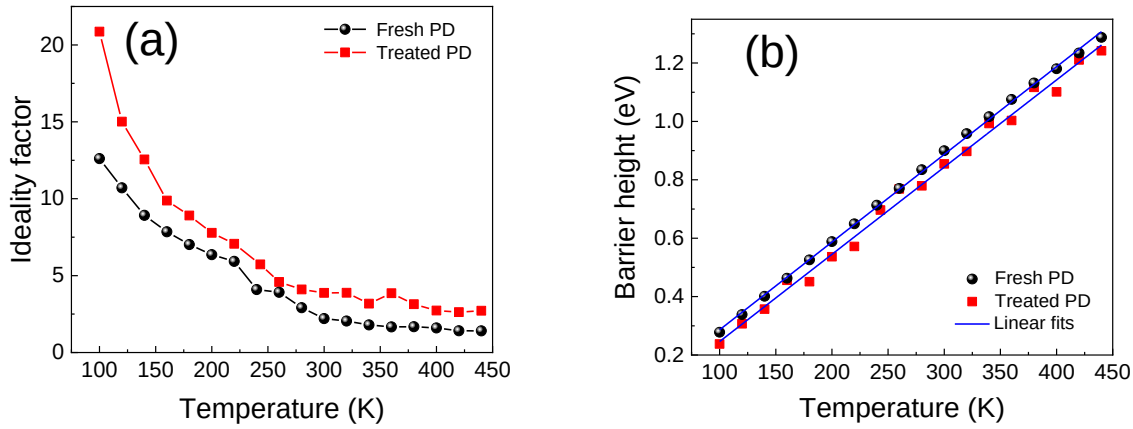

Fig. 5. Temperature dependence of (a) ideality factor, and (b) barrier height, obtained from *I–V* characteristics for fresh and treated PDs.

3.4. Analysis of the C–V characteristics

The change in the carrier concentration (N_d) during the stress can affect the degradation process strongly [15,19]. Therefore, quantitative analysis in the change of N_d during the stress is required to realize its clear scenario. In this work, to determine the value of N_d, we measured the *C–V* characteristics of both devices at room temperature using a frequency of 1 MHz and the results are shown in Fig. 6a. The slope of the best fit of the $1/C^2$ versus reverse bias plot is used to calculate the free carrier concentrations as illustrated in Fig. 6b. For the fresh PDs, the free carrier concentration of 4.1×10^{15} cm^{-3} is consistently uniform, as evidenced by the linear trend exhibited by the plot of $1/C^2$ versus applied bias. However, for the treated PDs, two lines are fitted to the *C–V* data, confirming the presence of two different free carrier concentrations of 1.6×10^{15} cm^{-3} and 5.2×10^{14} cm^{-3}. This decrease in N_d is probably related to the increase of the number of defects after stress. This will be confirmed in the DLTS section. However, for the treated PDs, a reduction of the capacitance can be observed, which points to reduced Space-Charges Regions (SCRs) in at least one of the SCRs and a widening of the involved SCRs. This reduction after stress can be attributed to an increase in defect-induced acceptor states, which is most likely to be the cause of a

reduction of charge states in pn-SCRs [15]. These defects can be generated during the stress leading to a carrier redistribution in the active region and the induced point defects generated during the degradation process are located within MQW region [19].

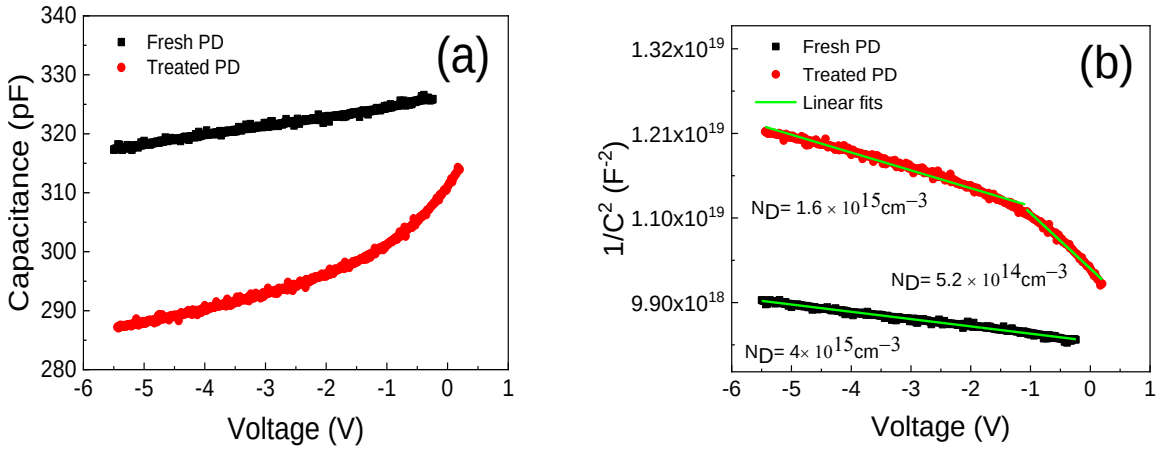

Fig. 6. (a) *C–V* plots at room temperature for fresh and treated PDs. (b) The plot of $1/C^2$ as a function of voltage.

To determine the presence and properties of defects in the investigated PD structures that can affect their degradation, we performed DLTS measurements for both untreated and treated PDs. DLTS technique has been previously employed to evaluate the effects of current stress on electrically active defects [32]. In the present work, the adopted experimental DLTS parameters are: a reverse bias, V_R = -0.5 V and -5 V, a filling pulse height, V_P = 0V, a filling pulse time, t_P = 1 msec, and a rate window of 500 s^{-1}. As illustrated in Fig. 7, the DLTS signals have been plotted against temperature for only the treated PDs over the scanned temperature range of 10-450 K. It is worth noting, no signals have been detected by DLTS in the fresh devices. This could be due to the fact that no defects are present in the fresh samples or they have very low concentrations beyond the detection limit of DLTS. However, the treated PDs exhibit only one negative peak at both reverse biases as shown in Fig. 7. It is evident in Fig. 7 that the amplitude of the DLTS signal increases with increasing reverse bias (away from the interface). This indicates that the concentration of the trap increases away from the interface.

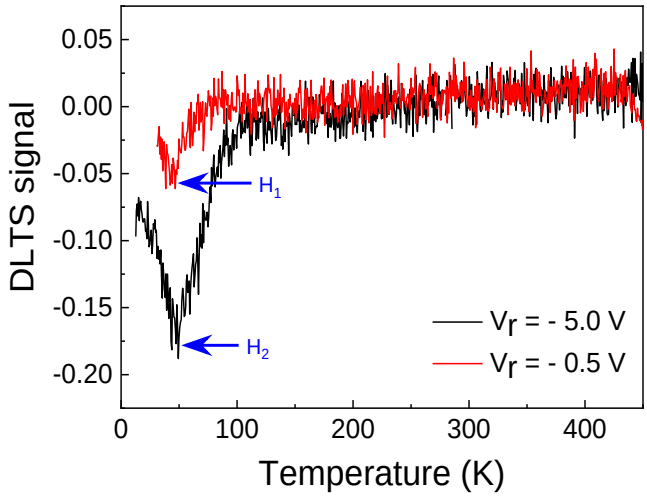

Fig. 7. DLTS spectra for the treated device at V_R = -0.5 V, and -5 V.

Since the DLTS peaks are broad, we have carried out Laplace DLTS (LDLTS) measurements to resolve these peaks [33]. Our LDLTS measurements show only one hole trap (H_1) and two hole traps (H_1, H_2) at reverse biases, V_R = -0.5 V and -5 V, respectively. The activation energies of these traps are determined from the Arrhenius plots as shown in Fig. 8. A summary of these traps parameters, including the activation energy, the trap concentrations, and the capture cross-section, is presented in Table 1.

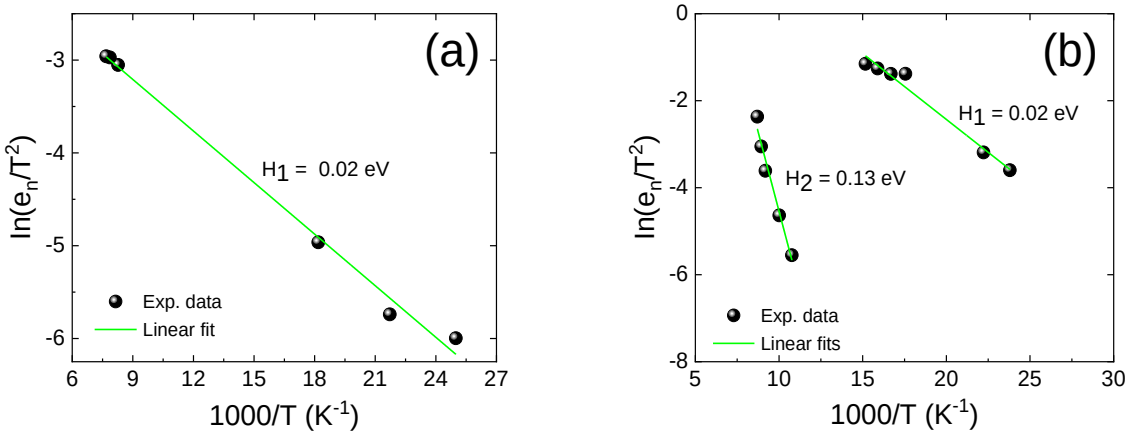

Fig. 8. Arrhenius plots for the treated device obtained from Laplace DLTS at (a) V_R= -0.5 V, and (b) V_R= -5 V.

Table 1.

Traps parameters for the treated device at V_R= (-0.5 and -5) V, V_P= 0V, and t_P = 1 msec.

Reverse bias (V)	Trap	Activation energy (eV)	Trap concentration (cm^{-3})	Capture cross-section (cm^2)
-0.5	H_1	0.020 ±0.001	5.5×10^{11}	8.2×10^{-23}
-5.0	H_1	0.020 ±0.001	1.5×10^{12}	1.4×10^{-20}
	H_2	0.13 ±0.01	1.8×10^{18}	9.0×10^{-18}

As shown in Table 1, the trap H_1 with an activation energy of 0.02 eV is observed in the treated device at both reverse biases (V_R = -0.5 V and -5 V), indicating that this trap exists near and away from the junction interface. A similar shallow trap (D1) with an activation energy of 0.07 eV has been reported in 100 mA stressed InGaN/GaN structure grown on SiC substrates [34]. This trap, which is found to be due to device degradation after current stress, may originate from the evolution of Mg complexes and the generation of NRCs during growth. This shallow trap has also been observed in AlGaN/InGaN/GaN heterostructures before current stress with similar activation energy (0.07 eV), however, no explanation was given regarding its possible origin [35]. In addition, the authors in Ref. [35] have not detected any deep traps in AlGaN/InGaN/GaN heterostructures. The capture cross-section of the H_1 trap at V_R = -0.5 V is 8.2×10^{-23} cm^2, whereas it is higher (1.4×10^{-20} cm^2) at V_R = -5 V. Its concentration at V_R = -0.5 V (near interface) and V_R = -5 V (away from interface) as determined from LDLTS is 1.5×10^{11} cm^{-3} and 5.5×10^{12} cm^{-3}, respectively. These results, which agree with the observed amplitude of the DLTS signal, confirm that the trap is more concentrated away from the interface of the junction.

The additional H_2 trap with an activation energy of 0.13 ±0.01 eV and concentration of 1.8×10^{18} cm^{-3} is observed in treated PDs only at a reverse base V_R = -5 V (away from the interface). A similar deep defect with activation energy of 0.12 eV, labeled as trap A, has been detected in unstressed and stressed devices at different direct currents of 50 mA and 100 mA [36]. It is consistent with the predictions of the presence of Mg-related shallow acceptors, including Mg_{Ga} and Mg-H_2 complexes, which can form p-type layers as a result of the breaking of the Mg-H chemical complexes due to high heating levels during the aging treatment [35]. This trap with activation energy in the range of 0.12-0.14 eV is observed in GaN/InGaN MQW structures as well which is

attributed to a freeze out of Mg acceptors [37,38]. Moreover, the generation of these traps can be attributed to current stress. The induced stress generates point defects or dislocations, which can cause the sub-threshold region to increase and the ideality factor also to increase after stress, indicating the generation of point defects or dislocations [23]. Furthermore, these defect induced acceptor state are most likely to be the cause of the reduction of the capacitance [15] and carrier redistribution [19].

Finally, to evaluate the sensitization performance of the detector, responsivity (R_λ), external quantum efficiency (η), and detectivity (D^*) are often considered [11]. Therefore, to get further insight into the effect of current stress on the spectral sensitivity of the detectors, we have estimated the values of R_λ, η, and D^* from the PCS results for fresh and treated PDs. It is noted that our device shows the highest value of R_λ at 382 nm (power of the light used: 10 μW). Hence, we have calculated the values of R_λ, η, and D^* at 382 nm. The estimated values of R_λ, η, and D^* in the fresh PDs are 0.266 A/W, 85.9%, and 4.32×10^{11} Jones, respectively. Interestingly, as a consequence of high current stress, the values of R_λ, η, and D^* decrease to 0.257 A/W, 82.6%, and 0.68×10^{11} Jones in the treated PDs. These results suggest that the generated defects in the device during the stress treatment ruin the photodetection capability of the detector significantly.

4. Conclusions

In summary, we have fabricated InGaN/GaN MQW UV-PDs with an Al_2O_3 passivation layer and systematically studied the root mechanisms that could account for the degradation of the device performances due to constant current stress by employing several combined optical and electrical measurements. The obtained EL spectra suggest that the EL intensity decreases by about 48% in the treated PD due to 200 mA of current stress over 340 hours. This indicates that more of the charge carriers are captured by the newly created defects in the active region. In the treated PD, the reduction in V_{OC} is much larger than J_{SC}, indicating that V_{OC} seems to be the leading degradation mechanism in our devices. The strong reduction in V_{OC} can be ascribed to the enhancement of the defect-related forward conduction processes in the treated PDs. The dark I–V measurements suggest that in the treated PDs, the dramatic increase of the reverse and forward leakage currents suggests that the parasitic leakage routes, which are usually prompted by severe point defects within or around the MQW, are activated largely during the stress treatment. Furthermore, the temperature dependence of I–V characteristics in the treated PDs suggests that within

100-440 K, the values of ideality factor (barrier height) are always higher (lower) than that of the fresh devices, indicating the existence of generation-recombination centers caused by the created defects. It is noteworthy that as the source of the leakage currents in treated PDs, two major trap levels with different activation energies are observed in the LDLTS spectra. However, based on our obtained results, we assume that the degradation mechanisms in the treated PDs are strongly associated with the activation of initially inactive defects, mainly Mg-related shallow acceptors, including Mg_{Ga} and Mg-H_2 complexes. The worsening of device performances is closely attributed to the activation of acceptor levels in treated PDs as confirmed by LDLTS analysis. Finally, due to the stress treatment, the sensitization performance of the detector decreases significantly in treated PDs, suggesting the generated defects in the device can ruin their photodetection performance largely.

CRediT authorship contribution statement

Pradip Dalapati: Conceptualization, Methodology, Device fabrication and characterizations, Degradation measurements, Data analysis, Writing – original draft. **Abdulaziz Almalki:** Methodology, Low-temperature measurements, LDLTS characterizations, Data analysis, Writing – original draft. **Sultan Alhassan:** Investigation. **Saud Alotaibi:** Investigation. **Maryam Al Huwayz:** Investigation. **Taiki Nakabayashi:** Device fabrication and characterizations, Formal analysis. **Takashi Egawa:** Resources, Validation, Writing – review & editing, Coordinated the work. **Makoto Miyoshi:** Resources, Validation, Writing – review & editing, Coordinated the work. **Mohamed Henini:** Conceptualization, Methodology, Resources, Validation, Writing – review & editing, Coordinated the work. All authors contributed by critically reading the manuscript.

Declaration of Competing Interest

The authors declare that they have no known competing financial interests or personal relationships that could have appeared to influence the work reported in this paper.

Appendix A. Supporting information

Supplementary data associated with this article can be found in the online version at xx

References

[1] D. Guo, H. Liu, P. Li, Z. Wu, S. Wang, C. Cui, C. Li, W. Tang, Zero-power-consumption solar-blind photodetector based on β-Ga_2O_3/NSTO heterojunction, ACS Appl. Mater. Interfaces 9 (2017) 1619−1628, https://doi.org/10.1021/acsami.6b13771.

[2] D. Han, K. Liu, Q. Hou, X.Chen, J. Yang, B. Li, Z. Zhang, L. Liu, D. Shen, Self-powered solar-blind $ZnGa_2O_4$UV photodetector with ultra-fast response speed, Sens. Actuators A Phys. 315 (2020) 112354−112360, https://doi.org/10.1016/j.sna.2020.112354.

[3] S. Podder, J. Bora, S. Thakur, D. Gogoi, B. Basumatary, S.M. Borah, N.C. Adhikary, A.R. Pal, Interband transition in plasmonic titanium nitride and its contribution towards ZnO based pyro-phototronic application, Mater. Chem. Phys. 275 (2022) 125290–125298, https://doi.org/10.1016/j.matchemphys.2021.125290.

[4] R.H. Horng, P.H. Huang, Y.S. Li, F.G. Tarntair, C.S. Tan, Reliability study on deep-ultraviolet photodetectors based on $ZnGa_2O_4$ epilayers grown by MOCVD, Appl. Surf. Sci. 555 (2021) 149657−14966, https://doi.org/10.1016/j.apsusc.2021.149657.

[5] L. Liu, C. Yang, A. Patane, Z. Yu, F. Yan, K. Wang, H. Lu, J. Li, L. Zhao, High-detectivity ultraviolet photodetectors based on laterally mesoporous GaN, Nanoscale 9 (2017) 8142−8148, https://doi.org/10.1039/C7NR01290J.

[6] P. Dalapati, K. Yamamoto, T. Kubo, T. Egawa, M. Miyoshi, Bias-controlled photocurrent generation process in GaN-based ultraviolet p–i–n photodetectors fabricated with a thick Al_2O_3 passivation layer, Optik 245 (2021) 167691−167696, https://doi.org/10.1016/j.ijleo.2021.167691.

[7] C. Xie, X.T. Lu, X.W. Tong, Z.X. Zhang, F.X. Liang, L. Liang, L.B. Luo, Y.C. Wu, Recent progress in solar-blind deep-ultraviolet photodetectors based on inorganic ultrawide bandgap semiconductors, Adv. Funct. Mater. 29 (2019) 1806006−18060045, https://doi.org/10.1002/adfm.201806006.

[8] S. Kim, J, Kim, Highly selective ozone-treated β-Ga_2O_3 solar-blind deep-UV photodetectors, Appl. Phys. Lett. 117 (2020) 261101−261106, https://doi.org/10.1063/5.0030400.

[9] H. Yang, Z. Ma, Y. Jiang, H. Wu, P. Zuo, B. Zhao, H. Jia, H. Chen, The enhanced photo absorption and carrier transportation of InGaN/GaN quantum wells for photodiode detector applications, Sci. Rep. 7 (2017) 43357−43362, https://doi.org/10.1038/srep43357.

[10] C.H. Kang, G. Liu, C. Lee, O. Alkhazragi, J.M. Wagstaff, K.H. Li, F. Alhawaj, T.K. Ng, J.S. Speck, S. Nakamura, S.P. DenBaars, B.S. Ooi, Semipolar ($20\overline{2}1$) InGaN/GaN micro-photodetector for gigabit-per-second visible light communication, Appl. Phys. Express 13 (2020) 014001−014005, https://doi.org/10.7567/1882-0786/ab58eb.

[11] P. Dalapati, K. Yamamoto, T. Egawa, and M. Miyoshi, Evaluation of high-performance, self-powered and wavelength-selective InGaN/GaN multiple quantum well UV photodetectors fabricated on sapphire substrate: Analysis of the influence of growth temperature, Sens. Actuators A Phys. 331 (2021) 113050−113060, https://doi.org/10.1016/j.sna.2021.113050.

[12] G. Moses, X. Huang, Y. Zhao, M. Auf der Maur, E.A. Katz, J.M. Gordon, InGaN/GaN multi-quantum-well solar cells under high solar concentration and elevated temperatures for hybrid solar thermal-photovoltaic power plants, Prog. Photovolt. Res. Appl. 28 (2020) 1167–1174, https://doi.org/10.1002/pip.3326.

[13] S.J. Leem, Y.C. Shin, E.H. Kim, C.M. Kim, B.G. Lee, Y. Moon, I.H. Lee, T. G. Kim, Optimization of InGaN/GaN multiple quantum well layers by a two-step varied-barrier-growth temperature method, Semicond. Sci. Technol. 23 (2008) 125039–125043, https://doi.org/10.1088/0268-1242/23/12/125039.

[14] P. Dalapati, S. Urata, T. Egawa, Investigation of AlGaN/GaN high electron mobility transistors on Silicon (111) substrates employing multi-stacked strained layer superlattice structures, Superlattice. Microst. 147 (2020) 106709–1067018, https://doi.org/10.1016/j.spmi.2020.106709.

[15] P. Dalapati, K. Yamamoto, T. Egawa, M. Miyoshi, Impact of current-induced degradation process on the electro-optical characteristics of InGaN/GaN multiple-quantum-well photodetectors fabricated on sapphire substrate, Appl. Phys. Lett. 118 (2021) 021101−021105, https://doi.org/10.1063/5.0027127.

[16] P. Dalapati, K. Yamamoto, T. Egawa, M. Miyoshi, Understanding the degradation mechanisms of InGaN/GaN multiple quantum well UV photodetectors submitted to different current stresses, Opt. Lett. 46 (2021) 3568−3571, https://doi.org/10.1364/OL.434920.

[17] M. Miyoshi, T. Nakabayashi, K. Yamamoto, P. Dalapati, Takashi Egawa, Improved epilayer qualities and electrical characteristics for GaInN multiple-quantum-well photovoltaic cells and their operation under artificial sunlight and monochromatic light illuminations, AIP Advances 11 (2021) 095208–0952015, https://doi.org/10.1063/5.0062346.

[18] M. Miyoshi, T. Tsutsumi, T. Kabata, T. Mori, T. Egawa, Effect of well layer thickness on quantum and energy conversion efficiencies for InGaN/GaN multiple quantum well solar cells, Solid-State Electron. 129 (2017) 29–34, http://dx.doi.org/10.1016/j.sse.2016.12.009.

[19] Z. Ma, A. Almalki, X. Yang, X. Wu, X. Xi, J. Li, S. Lin, X. Li, S. Alotaibi, M. Alhuwayz, M. Henini, L. Zhao, The influence of point defects on AlGaN-based deep ultraviolet LEDs, J. Alloy. Comp. 845 (2020) 156177–156182, https://doi.org/10.1016/j.jallcom.2020.156177.

[20] X. Huang, H. Fu, H. Chen, Z. Lu, I. Baranowski, J. Montes, T.H. Yang, B.P. Gunning, D. Koleske, Y. Zhao, Reliability analysis of InGaN/GaN multiquantum-well solar cells under thermal stress, Appl. Phys. Lett. 111 (2017) 233511–233515, https://doi.org/10.1063/1.5006650.

[21] A. Caria, C. De Santi, F. Zamperetti, X. Huang, H. Fu, H. Chen, Y. Zhao, A. Neviani, G. Meneghesso, E. Zanoni, M. Meneghini, GaN-based high-periodicity multiple quantum well solar cells: Degradation under optical and electrical stress, Microelectron. Rel. 114 (2020) 113802–113807, https://doi.org/10.1016/j.microrel.2020.113802.

[22] J.H. Werner, Schottky barrier and pn-junction I/V plots–Small signal evaluation, Appl. Phys. A 47 (1988) 291–300, https://doi.org/10.1007/BF00615935.

[23] Z. Ma, H. Cao, S. Lin, X. Li, L. Zhao, Degradation and failure mechanism of AlGaN-based UVC-LEDs, Solid-State Electron, 156 (2019) 92–96, https://doi.org/10.1016/j.sse.2019.01.004.

[24] P. Dalapati, N.B. Manik, A.N. Basu, Study of effective carrier lifetime and ideality factor of BPW 21 and BPW 34B photodiodes from above room temperature to liquid nitrogen temperature, Cryogenics 65 (2015) 10–15, http://dx.doi.org/10.1016/j.cryogenics.2014.10.002.

[25] B.G. Park, R. Maddaka, T.K.P. Nguyen, K. Rao Peta, Y.K. Noh, J.E. Oh, M.D. Kim, Effects of reduced internal electric field in InGaN/pseudo-AlInGaN multi-quantum-well on forward leakage current and photocurrent properties, J. Appl. Phys. 126 (2019) 045703–045709, https://doi.org/10.1063/1.5094201.

[26] M. Ravinandan, P. Koteswara Rao, V.R. Reddy, Analysis of the current–voltage characteristics of the Pd/Au Schottky structure on n-type GaN in a wide temperature range, Semicond. Sci. Technol. 24 (2009) 035004–0350010, https://doi.org/10.1088/0268-1242/24/3/035004.

[27] S. Zhu, C. Detavernier, F. Cardon, G.-P. Ru, X.-P. Qu, B.-Z. Li, Electrical characteristics of CoSi2/n-Si (100) Schottky barrier contacts formed by solid state reaction, Solid-State Electron. 44 (2000) 1807–1818, https://doi.org/10.1016/S0038-1101(00)00127-1.

[28] S. Chand, J. Kumar, Electron transport and barrier inhomogeneities in palladium silicide Schottky diodes, Appl. Phys. A 65 (1997) 497–503, https://doi.org/10.1007/s003390050614.

[29] J.M. Shah, Y.-L. Li, T. Gessmann, E.F. Schubert, Experimental analysis and theoretical model for anomalously high ideality factors (n≫ 2.0) in AlGaN/GaN pn junction diodes, J. Appl. Phys. 94 (2003) 2627–2630, https://doi.org/10.1063/1.1593218.

[30] D.S. Reddy, M.B. Reddy, N.N.K. Reddy, V.R. Reddy, Schottky barrier parameters of Pd/Ti contacts on N-type InP revealed from IVT and CVT measurements, J. Mod. Phys. 2 (2011) 113, https://doi.org/10.4236/jmp.2011.23018.

[31] V.R. Reddy, N.N.K. Reddy, Current transport mechanisms in Ru/Pd/n-GaN Schottky barrier diodes and deep level defect studies, Superlattice. Microst. 52 (3) (2012) 484–499, http://dx.doi.org/10.1016/j.spmi.2012.06.004.

[32] D. Lang, Deep-level transient spectroscopy: A new method to characterize traps in semiconductors, J. Appl. Phys. 45 (1974) 3023–3032, https://doi.org/10.1063/1.1663719.

[33] L. Dobaczewski, A. Peaker, K. Bonde Nielsen, Laplace-transform deep-level spectroscopy: The technique and its applications to the study of point defects in semiconductors, J. Appl. Phys. 96 (2004) 4689–4728, https://doi.org/10.1063/1.1794897.

[34] G. Meneghesso, S. Levada, R. Pierobon, F. Rampazzo, E. Zanoni, A. Cavallini, A. Castaldini, G. Scamarcio, S. Du, I. Eliashevich, Degradation mechanisms of GaN-based LEDs after accelerated DC current aging, in Digest. International Electron Devices Meeting, (2002) 103–106, https://doi.org/10.1109/IEDM.2002.1175789.

[35] M. Osiński, J. Zeller, P.C. Chiu, B. Scott Phillips, D.L. Barton, AlGaN/InGaN/GaN blue light emitting diode degradation under pulsed current stress, Appl. Phys. Let. 69 (1996) 898–900, https://doi.org/10.1063/1.116936.

[36] G. Salviati, F. Rossi, N. Armani, M. Pavesi, M. Manfredi, G. Meneghesso, E. Zanoni, A. Castaldini, A. Cavallini, Influence of long-term DC-aging and high power electron beam irradiation on the electrical and optical properties of InGaN LEDs, Eur. Phys. J. Appl. Phys. 27 (2004) 345–348, 2004, https://doi.org/10.1051/epjap:2004066.

[37] A.Y. Polyakov, N.M. Shmidt, N.B. Smirnov, I.V. Shchemerov, E.I. Shabunina, N.A. Tal'nishnih, I.-H. Lee, L.A. Alexanyan, S.A. Tarelkin, S.J. Pearton, Deep trap analysis in green light emitting diodes: Problems and solutions, J. Appl. Phys. 125 (2019) 215701–215708, https://doi.org/10.1063/1.5093723.

[38] A.Y. Polyakov, N.B. Smirnov, E.B. Yakimov, H.-S. Cho, J.H. Baek, A.V. Turutin, I.V. Shemerov, E.S. Kondratyev, I.-H. Lee, Deep electron traps responsible for higher quantum efficiency in improved GaN/InGanN light emitting diodes embedded with SiO_2 nanoparticles, ECS J. Solid State Sci. Tech. 5 (2016) Q274, https://doi.org/10.1149/2.0051612jss.